

Radiation-pressure-driven dust transport to galaxy halos at $z \sim 10$

Hiroiyuki Hirashita^{1*} and Akio K. Inoue^{2,3,4}

¹*Institute of Astronomy and Astrophysics, Academia Sinica, Astronomy-Mathematics Building, AS/NTU, No. 1, Sec. 4, Roosevelt Road, Taipei 10*

²*Department of Environmental Science and Technology, Faculty of Design Technology, Osaka Sangyo University, 3-1-1, Nakagaito, Daito, Osaka 5*

³*Department of Physics, School of Advanced Science and Engineering, Waseda University, 3-4-1, Okubo, Shinjuku, Tokyo 169-8555, Japan*

⁴*Waseda Research Institute for Science and Engineering, 3-4-1, Okubo, Shinjuku, Tokyo 169-8555, Japan*

Accepted XXX. Received YYY; in original form ZZZ

ABSTRACT

The origin of dust in galaxy halos or in the circum-galactic medium (CGM) is still a mystery. We investigate if the radiation pressure in high-redshift ($z \sim 10$) galaxies can efficiently transport dust to halos. To clarify the first dust enrichment of galaxy halos in the early Universe, we solve the motion of a dust grain considering radiation pressure, gas drag, and gravity in the vertical direction of the galactic disc. Radiation pressure is estimated in a consistent manner with the stellar spectra and dust extinction. As a consequence, we find that dust grains with radii $a \sim 0.1 \mu\text{m}$ successfully escape from the galactic disc if the ongoing star formation episode converts more than 15 per cent of the baryon content into stars and lasts $\gtrsim 30$ Myr, while larger and smaller grains are trapped in the disc because of gravity and gas drag, respectively. We also show that grain charge significantly enhances gas drag at a few–10 scale heights of the galactic disc, where the grain velocities are suppressed to $\sim 1 \text{ km s}^{-1}$. There is an optimum dust-to-gas ratio ($\sim 10^{-3}$) in the galactic disc and an optimum virial mass $\sim 10^{10}\text{--}10^{11} M_{\odot}$ for the transport of $a \sim 0.1 \mu\text{m}$ grains to the halo. We conclude that early dust enrichment of galaxy halos at $z \gtrsim 10$ is important for the origin of dust in the CGM.

Key words: dust, extinction — galaxies: evolution — galaxies: haloes — galaxies: high-redshift — galaxies: ISM — radiation: dynamics

1 INTRODUCTION

Dust is known to exist in a wide volume in the Universe, not only in the interstellar medium (ISM) but also in the circum-galactic and intergalactic medium (CGM and IGM) (e.g. Ménard et al. 2010). The dust content in galaxy halos (or the CGM; hereafter, we simply use words ‘halo’ to indicate the circum-galactic environment) gives us a clue to the transport of dust from the ISM to the IGM, since halos are the interface between the ISM and the IGM. Ménard et al. (2010) detected reddening in galaxy halos using the cross-correlation between the galaxy position and the reddening of background quasi-stellar objects (QSOs) for a large sample of galaxies taken by the Sloan Digital Sky Survey (SDSS; York et al. 2000). The median redshift of their sample is $z \sim 0.3$ (z denotes the redshift). They detected reddening up to a radius of several Mpc from the galaxy centre. Peek et al. (2015) applied basically the same method to nearby galaxies ($z \sim 0.05$), and found a similar radial profile of reddening to the one found in Ménard et al. (2010). Masaki & Yoshida

(2012) confirmed the observationally suggested large extent of dust distribution in galaxy halos by comparing their analytic halo model with Ménard et al. (2010)’s data.

Since dust in the CGM and IGM affects the opacity toward distant objects in the Universe (Aguirre 1999), it is important to clarify the origin and evolution of dust in the cosmic volume. Dust in galaxy halos is also of fundamental importance in the total dust budget in galaxies and in the Universe, since Ménard et al. (2010) estimate that the dust mass in a galaxy halo is on average comparable to that in a galaxy disc. Moreover, as Inoue & Kamaya (2003, 2004, 2010) argued, dust could affect the thermal state of the IGM through photoelectric heating. They constrained the grain size and the dust-to-gas ratio in the IGM using the observed thermal history of the IGM, although those two quantities are degenerate in such a way that small grains require smaller abundance of dust.

Dust forms and evolves mainly in the ISM through various processes (Asano et al. 2013). Since a galaxy is not a closed system, the ISM interacts with the CGM and IGM through outflow driven by supernovae (SNe) and active galactic nuclei (AGNs) (e.g., Veilleux et al. 2005),

* E-mail: hirashita@asiaa.sinica.edu.tw

and through inflow driven by cooling and/or gravity (e.g., Kereš et al. 2005). The outflow could also transport the interstellar dust to the CGM and IGM (Zu et al. 2011; McKinnon et al. 2016; Hou et al. 2017; Aoyama et al. 2018). The exchange of materials between the ISM and the CGM/IGM, thus, affects the dust abundances in both the ISM and the CGM/IGM.

Dust motion from the ISM to the CGM/IGM could also be induced by a non-hydrodynamical process. Radiation pressure from stars in a galaxy could also drive the interstellar dust outward, supplying the dust to the CGM and IGM. In spite of some theoretical calculations of this process (Ferrara et al. 1991; Bianchi & Ferrara 2005), it is generally difficult to directly simulate the dust motion on galactic (or larger) scales, since the decoupling between dust and gas (i.e. the multi-fluid nature) is essential. Bekki et al. (2015), using multi-component particle methods, have shown that the radial dust density profile is affected by radiation pressure, but they did not focus on the ejection of dust particles from the galactic disc to the halo. Therefore, the current understanding of the CGM and IGM dust abundances are primarily based on the hydrodynamical effects (i.e. dust motion driven by hydrodynamical outflows). Further studies are necessary to investigate dust transport by radiation pressure.

Barsella et al. (1989) considered radiation pressure, gas drag (friction), and gravity and calculated the force field around a galaxy. They found that graphite grains have an outward force field due to efficient radiation pressure; thus, they expected that graphite grains are expelled out of the galaxy. Davies et al. (1998) also considered the motion in the gravitational potential typical of a disc galaxy composed of stars, gas, dust and dark halo. They showed that dust grains with $a \sim 0.1 \mu\text{m}$ (a is the grain radius) can be ejected from the galactic disc but that the dust motion is sensitive to the disc opacity. Small grains with $a < 0.01 \mu\text{m}$ stay relatively near to the disc because they are inefficient in receiving radiation pressure (i.e. they have small absorbing and scattering efficiencies). Simonsen & Hannestad (1999) showed that the velocities of escaping grains from a galactic disc are not strongly dependent on the grain size. They also mentioned that small grains could be slowed down by gas drag if the gas density in the halo is as high as expected for high-redshift galaxies. Ferrara et al. (1991) investigated the motion of dust pushed by radiation pressure toward the halo in the gravitational potential and the gas density profile typical of nearby spiral galaxies. They showed that dust grains obtain velocities in excess of 100 km s^{-1} (see also Shustov & Vibe 1995), and that grains with $a \sim 0.1 \mu\text{m}$ survive against sputtering in the hot halo. Bianchi & Ferrara (2005), using the IGM density distribution at $z \sim 3$ in a cosmological simulation, showed that dust grains transported to the IGM contribute to the metal enrichment there through sputtering. They argued that large ($a \gtrsim 0.1 \mu\text{m}$) grains are preferentially injected in the low-density IGM, since smaller grains are decelerated by gas drag in denser regions near galaxies.

The above studies focus on relatively low redshifts. In considering the origin of dust in the IGM, systematic studies starting from high redshift are crucial. Moreover, recent sensitive submillimetre and millimetre observations by ALMA have found some dusty ‘normal’ galaxies at $z > 7$ (Watson et al. 2015; Laporte et al. 2017; Hashimoto et al.

2019; Tamura et al. 2019). These galaxies could be the first sources of the dust in the IGM and CGM. This means that the first enrichment of dust on a wide scale in the Universe could have occurred at $z \gtrsim 7$. The above previous studies did not target such high redshift galaxies. Thus, it is worth investigating dust ejection from galaxies at $z \gtrsim 7$ as the ‘first’ dust sources in the CGM and IGM.

We expect that high-redshift galaxies manifest some differences in radiation-pressure-driven dust motion from low-redshift ones. A higher matter density at high redshift would cause stronger gravity. Since gravity could counteract radiation pressure, dust grains, especially large ones, may not efficiently escape out of the galactic disc. The higher baryon density potentially causes stronger gas drag; thus, the grain velocities may become slower or the grains could even be trapped in the galactic disc. On the other hand, if star formation occurs in a compact region, the stellar surface brightness (intensity) becomes higher. This makes radiation pressure stronger. The lower metal content in high-redshift galaxies could predict stronger radiation pressure because less fraction of stellar light is extinguished. Denser gas density, on the contrary, will raise the extinction optical depth.

The goal of this paper is to examine the above effects regarding dust motion systematically for galaxies at redshifts as high as $z \gtrsim 7$. We put particular focus on whether or not the dust grains in the galactic disc (or the ISM) are successfully pushed and transported to the galaxy halo (or CGM) by radiation pressure in spite of the counteracting forces (gas drag and gravity). This transport is referred to as *grain escape*. As mentioned above, it is not easy to solve dust dynamics in a cosmological simulation, although there are some codes that are capable of treating gas–grain decoupling (Bekki et al. 2015; McKinnon et al. 2018). Thus, some analytic approaches that focus on high-redshift galaxies would be useful. In this paper, we analytically model the three relevant forces – radiation pressure, gas drag, and gravity – consistently, focusing on relevant redshift scalings. In this way, we will be able to address the importance of radiation pressure on the dust motion in a physical condition typical of high-redshift galaxies, although we apply some simplifications to make the problem analytically tractable. This paper also provides a useful step toward future direct simulations of dust motion or a viable tool to be used in semi-analytic galaxy evolution models. We also neglect small-scale structures in galactic disc; thus, this work is complementary to the studies that focus on radiation feedback on small scales such as H II regions (e.g. Akimkin et al. 2015, 2017; Ishiki et al. 2018).

The paper is organized as follows. We formulate the model in Section 2. We show the results in Section 3. We further discuss the model predictions and their implications in Section 4. Finally we conclude in Section 5. Throughout this paper, we adopt $H_0 = 70 \text{ km s}^{-1} \text{ Mpc}^{-1}$ (the Hubble constant at $z = 0$), $\Omega_{\text{M}} = 0.3$ (the matter density normalized to the critical density), $\Omega_{\Lambda} = 0.7$ (the cosmological constant), and $\Omega_{\text{b}} = 0.04$ (the baryon density normalized to the critical density) for the cosmological parameters.

2 MODEL

We construct a framework that describes the dust motion in a high-redshift galaxy with an explicit dependence on the redshift. The entire formulation is composed of a galaxy model, a hydrostatic model of star-forming gas, and a dynamical model for a dust grain. We target high-redshift galaxies which experience the first major star formation in a gas-rich environment. For simplicity, we neglect the change of grain radius by sputtering. This is valid for most of the virial mass range of interest, since the virial temperature is lower than 10^6 K.¹

We treat a dust grain as a test particle, and consider its motion equation. In this paper, we consider silicate as a representative dust species unless otherwise stated, but we also consider graphite to examine the material dependence of the grain motion. The grain is assumed to be spherical with a uniform material density denoted as s . The grain mass m is estimated as

$$m = \frac{4}{3}\pi a^3 s. \quad (1)$$

We give the grain radius as a free parameter. We adopt $s = 3.5$ and 2.24 g cm⁻³ (Weingartner & Draine 2001b) for silicate and graphite, respectively. We fix the gas structure; that is, we neglect the feedback caused by dust motion through gas drag. This is justified since the stellar surface brightnesses (densities) of galaxies we consider in this paper are much lower than the value at which the radiation pressure affects the gas structure (Crocker et al. 2018).

2.1 Galaxy model

Here we provide the basic galaxy structures based on which we estimate relevant forces (gravity, gas drag, and radiation pressure). The gravitational potential is broadly determined by the matter density as a result of the cosmological structure formation. For gas drag, we need to model a gravitational equilibrium structure of the gas component. For radiation pressure, we consider the luminosity of stars formed from the gas component. We explain the galaxy model in what follows.

We consider a galaxy with virial mass M_{vir} formed at redshift z_{vir} (i.e. M_{vir} and z_{vir} are given parameters). We expect that this object has a virial radius of r_{vir} described by (e.g. Kitayama & Suto 1996)

$$\frac{4}{3}\pi r_{\text{vir}}^3 \Delta_c \rho_{\text{c}0} \Omega_{\text{M}} (1 + z_{\text{vir}})^3 = M_{\text{vir}}, \quad (2)$$

where Δ_c is the overdensity of a gravitationally bound object normalized to the mean cosmic matter density, and $\rho_{\text{c}0} \equiv 3H_0^2/(8\pi G)$ is the critical density of the Universe at $z = 0$ (G is the gravitational constant). We adopt $\Delta_c = 200$

¹ Thermal sputtering is negligible at temperature $< 10^6$ K (Draine & Salpeter 1979). The virial temperature is estimated in Appendix A (equation A3), and is lower than 10^6 K for $M_{\text{vir}} \lesssim 10^{11} M_{\odot}$. As shown later, galaxies with $M_{\text{vir}} \sim 10^{10}$ – $10^{11} M_{\odot}$ are important for grain escape. Also, objects with $M_{\text{vir}} > 10^{11} M_{\odot}$ are rare at $z \gtrsim 10$ (e.g. Reed et al. 2003). As we show later, the grain velocity is less than 100 km s⁻¹ in the height (ζ introduced later) range of interest (\lesssim several tens of pc); thus, nonthermal sputtering can be neglected as well.

(e.g. Peebles 1980; Kitayama & Suto 1996). Because of the dissipative nature, the cooled portion of the gas in the galaxy halo is expected to be settled in a disc whose radius denoted as r_{disc} is determined by the initial angular momentum (e.g. Ferrara et al. 2000). In this situation, the typical surface density of the baryon in the disc (Σ_{b}) is estimated as

$$\Sigma_{\text{b}} = \frac{(\Omega_{\text{b}}/\Omega_{\text{M}})f_{\text{disc}}M_{\text{vir}}}{\pi q_{\text{disc}}^2 r_{\text{vir}}^2}, \quad (3)$$

where $q_{\text{disc}} \equiv r_{\text{disc}}/r_{\text{vir}}$ is the disc radius normalized to the virial radius, f_{disc} is the fraction of baryon contained in the disc [fraction $(1 - f_{\text{disc}})$ is contained in the halo; see equation 10] and the baryon fraction in the galaxy is assumed to be equal to the cosmic mean ($\Omega_{\text{b}}/\Omega_{\text{M}}$). Considering the conservation of angular momentum with a typical value of the spin parameter (0.04; Barnes & Efstathiou 1987), we obtain $q_{\text{disc}} \approx 0.18$ (Ferrara et al. 2000). Note that we give M_{vir} and z_{vir} in our model, and eliminate r_{vir} in equation (3) using equation (2). As a consequence, we obtain Σ_{b} for a given set of M_{vir} and z_{vir} . We fix $q_{\text{disc}} = 0.18$ unless otherwise stated, but vary f_{disc} later. For reference, we give the numerical estimates of r_{vir} and r_{disc} in equations and (A1) and (A2), respectively, of Appendix A. The uncertainty caused by the assumed geometry of gas and stars can be examined practically by changing q_{disc} . For example, if the gas and stars are spherically distributed in a compact manner, this case is approximated by a small q_{disc} . However, the variation of q_{disc} does not affect our conclusion (Section 4.5).

We concentrate on the physical properties perpendicular to the disc, since we are interested in the dust motion toward the galaxy halo. In this way, the problem is reduced to one dimension. We expect that our treatment gives a representative estimate even in the presence of complicated structures as long as we are interested in the dust motion from the ISM (i.e. a concentration of the baryonic component) to the outer direction. We leave the complexity arising from multi-dimensional structures for future work.

We consider stars as radiation sources. We introduce the star formation efficiency ϵ_{\star} , which expresses the fraction of gas converted into stars. With this quantity, the surface densities of stars (Σ_{\star}) and gas (Σ_{gas}) are written, respectively, as

$$\Sigma_{\star} = \epsilon_{\star}\Sigma_{\text{b}}, \quad \text{and} \quad \Sigma_{\text{gas}} = (1 - \epsilon_{\star})\Sigma_{\text{b}}. \quad (4)$$

Precisely speaking, a part of Σ_{\star} has been returned into the gas; thus, Σ_{\star} is not exactly the total mass of the surviving stars. We should keep in mind that our definition of the stellar mass is the integral of the past star formation rate (SFR). In solving radiation transfer and dynamics below, we assume homogeneity in the directions parallel to the disc plane. We use coordinate ζ in this direction with $\zeta = 0$ corresponding to the disc midplane. We also approximate that the homogeneous disc extends to the infinity. This assumption is equivalent to $\zeta \ll r_{\text{disc}}$, which holds for our calculations.

2.2 Gravity

For the gravitational field, we need to consider the contributions from both baryon and dark matter. Here we formulate the gravitational field effectively including these two components based on the formula applied to the Galaxy. Since

we are only interested in the vertical direction of the baryonic disc, we employ the following functional form for the gravitational field (Franco et al. 1991):

$$g_\zeta = \beta \tanh\left(\frac{\zeta}{H_M}\right), \quad (5)$$

where $\beta = 4\pi G H_M \rho_{\text{tot}}(0)$ [$\rho_{\text{tot}}(0)$ is the total mass density at the midplane], and H_M is the mass scale height. This function is valid for an isothermal self-gravitating disc. Franco et al. (1991) used this gravity model for the structure of the Galactic disc (see also Ferrara 1993), and we adopt it for the sake of simplicity. This expression is still modified to include appropriate scaling of H_M and β with virial mass and redshift as we explain below.

Since $H_M \rho_{\text{tot}}(0)$ roughly gives the matter surface density, we expect that it has the same scaling as $M_{\text{vir}}/r_{\text{vir}}^2 \propto M_{\text{vir}}^{1/3}(1+z_{\text{vir}})^2$ [note that $r_{\text{vir}} \propto M_{\text{vir}}^{1/3}(1+z_{\text{vir}})^{-1}$ from equation (2), and recall that we give constant parameters M_{vir} and z_{vir}]. Therefore, we assume that $\beta \propto M_{\text{vir}}^{1/3}(1+z_{\text{vir}})^2$. This scaling reflects the tendency of stronger gravitational field in higher-redshift galaxies as a result of higher matter density. Assuming $\rho_{\text{tot}}(0) \propto (1+z_{\text{vir}})^3$, we obtain $H_M \propto \beta/\rho_{\text{tot}}(0) \propto M_{\text{vir}}^{1/3}(1+z_{\text{vir}})^{-1}$. Based on the above scaling relations, we adopt the following expressions for β and H_M :

$$\beta = \beta_\odot (M_{\text{vir}}/10^{12} M_\odot)^{1/3} (1+z_{\text{vir}})^2, \quad (6)$$

$$H_M = H_{M\odot} (M_{\text{vir}}/10^{12} M_\odot)^{1/3} (1+z_{\text{vir}})^{-1}, \quad (7)$$

where the solar neighbourhood values (β_\odot and $H_{M\odot}$) are used to give local calibrations. We adopt $\beta_\odot = 3.07 \times 10^{-9} \text{ cm s}^{-2}$ and $H_{M\odot} = 250 \text{ pc}$ (de Boer 1991; Ferrara 1993). In the normalization, we assume that the Milky Way has established the current virial mass ($\sim 10^{12} M_\odot$; Trimble 2000) at $z \sim 0$. In reality, the density structure within the galaxy is complex because of non-spherical distribution of dark matter and complicated structure formation of gas and stars. Although there are uncertainties in the values of β and H_M , the above simple scaling relations (as a function of z_{vir} and M_{vir}) are useful to examine the systematic difference in gravitational potential from the preceding work in the solar neighbourhood.

2.3 Hydrostatic equilibrium of the gas

The density stratification of gas is important for the grain motion, since it affects drag and extinction as a function of ζ . The gas density in the disc, $\rho_{\text{disc}}(\zeta)$, is determined by considering the hydrostatic condition:

$$\sigma^2 \frac{d\rho_{\text{disc}}(\zeta)}{d\zeta} + \rho_{\text{disc}}(\zeta) g_\zeta = 0, \quad (8)$$

where σ denotes the effective sound speed including the turbulent velocity. For simplicity, we assume σ to be constant. We solve this equation with a boundary condition of $\rho_{\text{disc}}(\zeta = 0) \equiv \rho_0$ and adjust ρ_0 to satisfy the total column density as

$$\int_0^\infty \rho_{\text{disc}}(\zeta) d\zeta = \Sigma_{\text{gas}}. \quad (9)$$

The density declines exponentially at large ζ . In reality, we expect that the gas density at large ζ approaches to a

value expected for the gaseous halo. We use the following mean gas density $\rho_{\text{g,halo}}$ for the halo:

$$\rho_{\text{g,halo}} = \frac{(1-f_{\text{disc}})M_{\text{vir}}\Omega_b/\Omega_M}{\frac{4}{3}\pi r_{\text{vir}}^3}. \quad (10)$$

The final gas density profile is determined by

$$\rho(\zeta) = \max[\rho_{\text{disc}}(\zeta), \rho_{\text{g,halo}}]. \quad (11)$$

We also use the hydrogen number density, n_{H} , which is related to ρ as

$$n_{\text{H}} = \rho/(\mu_{\text{H}} m_{\text{H}}), \quad (12)$$

where $\mu_{\text{H}} (= 1.4)$ is the gas mass per hydrogen, and m_{H} is the mass of hydrogen atom. The velocity dispersion σ is a given parameter. Unless otherwise stated, we assume that $\sigma = 10 \text{ km s}^{-1}$, which is the typical velocity dispersion of the warm neutral medium in the Galactic disc (e.g. Spitzer 1978) and in nearby galaxies (e.g. Young & Lo 1997).

For convenience, we define the typical scale height, $H_{\text{g}0}$, as (see also equation 6)

$$H_{\text{g}0} \equiv \frac{\sigma^2}{\beta} \simeq 4.0 \left(\frac{M_{\text{vir}}}{10^{10} M_\odot}\right)^{-1/3} \left(\frac{1+z_{\text{vir}}}{11}\right)^{-2} \text{ pc}. \quad (13)$$

This is much thinner than the discs of the Galaxy and nearby galaxies (e.g. Yim et al. 2014; Nakanishi & Sofue 2016), which is a consequence of the redshift dependence of the gravity (recall that higher densities at higher redshifts lead to stronger gravity). In reality, the disc structure would be disturbed by H II regions and SNe, but the above static dense disc would give strong gas drag (and a conservative estimate of grain escape from the disc). We also define the exponential height as ζ at which the density drops 1/e times the central value. Because the gravity is weak at $\zeta \ll H_{\text{g}0}$, the actual scale height (exponential height) is larger than $H_{\text{g}0}$ by a factor of ~ 2 .

2.4 Radiation pressure

For the radiation field, we consider the emission from stars. To calculate the spectral energy distribution (SED) of the stellar component, we adopt Bruzual & Charlot (2003). The SED per stellar mass (ℓ_ν) is calculated with a constant SFR with a duration (age) of t_\star . To simplify the computation, we fix the stellar SED (do not vary the SED along time t). The calculation is valid for $t \lesssim t_\star$ (otherwise, the time is contradictory with the stellar age). Instead of modeling the complication in the past star formation history, we vary t_\star . For a test, we also examined the instantaneous burst with an age of t_\star , but we found that radiation pressure is too weak to push the grains to the halo if $t_\star \gtrsim 30 \text{ Myr}$. Therefore, we confirmed that an ongoing star formation activity is essential for radiation pressure to work effectively. The stellar metallicity is assumed to be 0.004 ($\sim 1/5 Z_\odot$; considering low metallicity at high redshift) and the Chabrier initial mass function (Chabrier 2003) with a stellar mass range of 0.1–100 M_\odot is adopted. There are some degeneracies among the parameters, but the age has a largest impact on the SED. Thus, we only move t_\star for the stellar properties in this paper.

We estimate the stellar surface brightness SED as a

function of frequency ν (denoted as $\Sigma_{\star\nu}$) using the stellar surface density in equation (4):

$$\Sigma_{\star\nu} = \Sigma_{\star} \ell_{\nu}. \quad (14)$$

Recall that ℓ_{ν} is the SED per stellar mass calculated above. For simplicity, we assume that the stars are concentrated in the midplane (i.e., at $\zeta = 0$). This assumption does not affect our conclusion since we are mainly interested in the grain motion at higher ζ than the scale height. In this case, the radiation transfer equation for the intensity $I_{\nu} = I_{\nu}(\zeta, \mu)$ is written using the gas density profile $\rho(\zeta)$ in Section 2.3 as

$$\mu \frac{dI_{\nu}}{d\zeta} = -\kappa_{\text{g,abs}}(\nu)\rho(\zeta)I_{\nu} + \frac{1}{4\pi}\Sigma_{\star\nu}\delta(\zeta), \quad (15)$$

where $\mu = \cos\theta$ (θ is the angle from the ζ direction), $\kappa_{\text{g,abs}}(\nu)$ is the mass absorption coefficient of the gas (the opacity is contributed from the dust) at frequency ν , and $\delta(\zeta)$ is Dirac's delta function. For simplicity, we neglect scattering. This could cause an underestimate of dust optical depth by a factor of 2 or less; however, the difference in the grain opacity caused by various grain size distributions has a comparable uncertainty. Moreover, we consider a large range for the dust abundance, for which we do not discuss the precision within factor 3. Therefore, neglecting scattering does not affect our conclusions in this paper. By solving this equation, we obtain

$$I_{\nu}(\zeta, \mu) = \frac{\Sigma_{\star\nu}}{4\pi\mu} \exp\left(-\frac{1}{\mu} \int_0^{\zeta} \kappa_{\text{g,abs}}(\nu)\rho(\zeta') d\zeta'\right). \quad (16)$$

The mass absorption coefficient $\kappa_{\text{g,abs}}(\nu)$ is estimated as

$$\kappa_{\text{g,abs}}(\nu) = \mathcal{D} \frac{\int_0^{\infty} \pi a^2 Q_{\text{abs}}(a, \nu) n(a) da}{\int_0^{\infty} \frac{4}{3} \pi a^3 s n(a) da}, \quad (17)$$

where \mathcal{D} is the dust-to-gas mass ratio (hereafter simply referred to as the dust-to-gas ratio), $Q_{\text{abs}}(a, \nu)$ is the absorption cross-section normalized to the geometrical cross-section, and $n(a)$ is the grain size distribution [$n(a) da$ is proportional to the number of grains with radii between a and $a + da$; the normalization of $n(a)$ cancels out in the above expressions]. The grain size distribution is assumed to be described by a power-law suggested by Mathis et al. (1977, hereafter MRN):

$$n(a) = \begin{cases} Ca^{-3.5} & \text{if } a_{\text{min}} < a < a_{\text{max}}, \\ 0 & \text{otherwise,} \end{cases} \quad (18)$$

where C is the normalization constant, which cancels out as mentioned above. We adopt $a_{\text{min}} = 0.005 \mu\text{m}$ and $a_{\text{max}} = 0.25 \mu\text{m}$ according to MRN. The absorption cross-section factor $Q_{\text{abs}}(a, \nu)$ is calculated using the Mie theory (Bohren & Huffman 1983) with the same optical constants as adopted in Weingartner & Draine (2001b). We adopt silicate, which is consistent with the extinction curve in the Small Magellanic Cloud (Pei 1992). The changes of the grain size distribution and the grain species cause variations in the grain opacity. As shown later, the result is sensitive to the dust-to-gas ratio, while we confirmed that the grain size distribution and the grain species cause a subdominant variation to the results. For example, the change of a_{min} to a larger value (such as $0.1 \mu\text{m}$) causes a drop of the dust opacity within a factor of 2, which is compensated by the increase of \mathcal{D} by the same factor (at most factor 2). We concentrate on the variation of \mathcal{D} in this paper.

Finally, we estimate the radiation force on the dust grain of interest. The radiation force as a function of a and ζ , $F_{\text{g,rad}}(a, \zeta)$, is calculated as

$$F_{\text{d,rad}}(a, \zeta) = \frac{2\pi}{c} (\pi a^2) \int_0^{\infty} d\nu \int_0^1 d\mu Q_{\text{rad}}(a, \nu) I_{\nu}(\zeta, \mu) \mu^2, \quad (19)$$

where $Q_{\text{rad}}(a, \nu)$ is the grain cross-section for radiation pressure normalized to the geometric cross-section. This quantity is evaluated as $Q_{\text{rad}}(a, \nu) = Q_{\text{abs}}(a, \nu) + (1 - g_s)Q_{\text{sca}}(a, \nu)$, where g_s is the scattering asymmetry factor. The relevant quantities are calculated by the Mie theory.

Weingartner & Draine (2001c) studied other forces due to photoelectron emission and the photodesorption of adatoms, which could be important in anisotropic radiation fields. The force due to photoelectron emission is not efficient if the grain potential is high: since Coulomb drag caused by highly positive grain charges is the most important factor in determining grain escape as shown later, photoelectron emission is not relevant in our context. Moreover, this force is at most only comparable to radiation pressure. Thus, taking photoelectron emission into account does not change our conclusion significantly. The photodesorption of adatoms could have a large impact on large ($a \gtrsim 0.1 \mu\text{m}$) grains, and would help further to push such large grains toward high ζ . Thus, our estimates could be conservative for grain escape: as shown later, grains with $a \sim 0.1 \mu\text{m}$ escape out of the galactic disc. For this case, the desorption force makes grain escape even easier. For grains as large as $a \sim 1 \mu\text{m}$, whether or not photodesorption helps grains escape from the disc is worth investigating, but to do this, further modeling of the physical conditions in the disc (gas temperature, ionization degree, etc.) is required. We leave this problem for future work.

2.5 Gas drag

For the grain motion, gas drag is also important. We refer to Draine & Salpeter (1979) for the estimate of gas drag. The drag force, F_{drag} , is expressed as (see also McKee et al. 1987)

$$F_{\text{drag}} = F_{\text{drag,direct}} + F_{\text{drag,plasma}}, \quad (20)$$

where the first and second terms on the right-hand side represent the effects of direct collisions and Coulomb interaction, respectively. These two terms are evaluated as

$$F_{\text{drag,direct}} \approx \pi a^2 |v_{\zeta}| \rho \left(v_{\zeta}^2 + \frac{128}{9\pi} \frac{k_{\text{B}} T}{\mu_{\text{H}} m_{\text{H}}} \right)^{1/2}, \quad (21)$$

$$F_{\text{drag,plasma}} \approx 4\pi a^2 k_{\text{B}} T \phi^2 \ln \Lambda \sum_i n_i Z_i^2 H(s_i), \quad (22)$$

where v_{ζ} is the grain velocity in the ζ direction, k_{B} is the Boltzmann constant, T is the gas temperature (fixed at the beginning of Section 3), ϕ is the grain electric potential energy normalized to the gas thermal energy (see below), $\ln \Lambda$ is the Coulomb logarithm, n_i is the number density of ion species i (we consider hydrogen and helium with a number ratio of 9 : 1 with both species in the first ionized state with an ionized fraction of f_{ion}), Z_i is the charge in units of electron charge (e), and $H(s_i)$ is a function of s_i defined below. The normalized grain potential is estimated by

$$\phi = \frac{Z_{\text{d}} e^2}{a k_{\text{B}} T}, \quad (23)$$

while the Coulomb logarithm and the function H are, respectively, given by

$$\Lambda = \frac{3}{2ae\phi} \left(\frac{k_{\text{B}}T}{\pi n_e} \right)^{1/2}, \quad (24)$$

where n_e is the electron number density (we assume $n_e = 1.1f_{\text{ion}}n_{\text{H}}$ considering the contribution from helium, where f_{ion} is the ionization degree), and

$$H(s_i) \simeq s_i \left(\frac{3}{2} \sqrt{\pi} + 2s_i^3 \right)^{-1} \quad (25)$$

with

$$s_i \equiv \frac{m_i v_{\zeta}^2}{2k_{\text{B}}T} \quad (26)$$

(m_i is the mass of ion species i), following the approximated expression derived by [Draine & Salpeter \(1979\)](#). Note that in the above definition, F_{drag} is always positive. Thus, considering the direction, the drag force is expressed as $-F_{\text{drag}}v_{\zeta}/|v_{\zeta}|$. We discuss and fix f_{ion} at the beginning of Section 3.

For the grain charge, we consider the balance between photoelectric charging and collisional charging following [Inoue & Kamaya \(2003\)](#). The collisional charging rate by particle species i (H, He, or e), R_i , is estimated for the Maxwellian velocity distribution as (e.g. [Draine & Sutin 1987](#))

$$R_i = \pi a^2 Z_i S_i n_i \left(\frac{8k_{\text{B}}T}{\pi m_i} \right)^{1/2} g(x), \quad (27)$$

where S_i is the sticking coefficient (assumed to be unity), $x \equiv Z_i \phi$, and

$$g(x) = \begin{cases} 1 - x & \text{for } Z_d Z_i \leq 0, \\ \exp(-x) & \text{for } Z_d Z_i > 0. \end{cases} \quad (28)$$

We neglect the image potential, since the grains are highly positively charged in the region where the Coulomb drag force is important. The photoelectric charging rate, on the other hand, is given by (e.g. [Draine 1978](#))

$$R_{\text{pe}} = \pi a^2 \int_0^{\infty} Q_{\text{abs}}(a, \nu) Y_{\nu}(a, Z_d) \frac{4\pi J_{\nu}}{h\nu} d\nu, \quad (29)$$

where Y_{ν} is the photoelectric yield, J_{ν} is the mean intensity averaged over the solid angle (estimated below), and h is the Planck constant. We estimate Y_{ν} based on [Weingartner & Draine \(2001a\)](#). The mean intensity is calculated as

$$J_{\nu} = \frac{1}{2} \int_0^1 I_{\nu}(\mu) d\mu. \quad (30)$$

Since the radiation only comes from the lower hemisphere, the integration range is from 0 to 1 (i.e. $I_{\nu} = 0$ for $-1 \leq \mu < 0$).

2.6 Motion equation of a dust grain

The motion equation of a dust grain is written as

$$m \frac{dv_{\zeta}}{dt} = F_{\text{d,rad}} - mg_{\zeta} - F_{\text{drag}} \frac{v_{\zeta}}{|v_{\zeta}|}. \quad (31)$$

Each term on the right-hand side is evaluated in one of the previous subsections. We adopt the boundary condition $v_{\zeta} =$

Table 1. Parameters.

Parameter	units	fiducial value	minimum	maximum
M_{vir}	M_{\odot}	10^{10}	10^8	10^{12}
z_{vir}		10	6	14
ϵ_{\star}		0.3	0.1	0.5
t_{\star}	Myr	30	10	100
a	μm	0.1	0.01	1
\mathcal{D}		10^{-3}	10^{-4}	10^{-2}

0 at $\zeta = 0$, but this is not important because the grain velocity at low ζ is determined by the equilibrium value (v_{ζ} such that $dv_{\zeta}/dt = 0$). We comment on the effect of varied initial velocities in Section 4.5.

Since the drag time-scale could be extremely short, we do not adopt an explicit discretization method for the time. We discretize the coordinate ζ to solve equation (31) and determine the grain motion iteratively between the two grid points (the discrete i th grid point is denoted as ζ_i). The width between the grid points are set as a few per cent of the typical scale height estimated in equation (13). From the velocity at ζ_i to ζ_{i+1} , we apply an analytic solution based on the solution at ζ_i and update the grain velocity at ζ_{i+1} . This velocity is used for the next iteration. We repeat this until the velocity at ζ_{i+1} converges. This iterative procedure stabilizes the obtained solution under a fixed spatial grid.

2.7 Varied parameters

There are some free parameters whose values should be specified. The parameters are categorized into two types: one is related to galaxies, and the other to dust. In what follows, we explain the range of the parameter values we adopt in this paper. The varied parameters are summarized in Table 1.

For the galaxy model, we move M_{vir} , z_{vir} , ϵ_{\star} , and t_{\star} . We are interested in the dust enrichment at high redshift $z \gtrsim 7$, where we already know that dusty galaxies existed as mentioned in the Introduction; thus, we examine $z_{\text{vir}} \sim 10$ ($z_{\text{vir}} = 6\text{--}14$). We consider $M_{\text{vir}} = 10^8\text{--}10^{12} M_{\odot}$, which covers the virial masses of the objects contributing to high-redshift star formation activities (e.g. [Ciardi et al. 2000](#)). For the star formation efficiency, we survey a range of $\epsilon_{\star} = 0.1\text{--}0.5$. As we find below, if $\epsilon_{\star} \leq 0.1$, dust is not pushed efficiently by radiation pressure. For t_{\star} , we examine 10, 30, and 100 Myr. We fix $f_{\text{disc}} = 0.5$ because of the degeneracy with ϵ_{\star} . Note that $f_{\text{disc}}\epsilon_{\star}$ is the fraction of the total baryonic mass converted into stars.

For the grain parameters, we vary a and \mathcal{D} . We consider a range of $a = 0.01\text{--}1 \mu\text{m}$, which roughly covers the grain sizes in the ISM (e.g. MRN). For $a \lesssim 0.01 \mu\text{m}$, as shown later, the grains are effectively trapped in the galactic disc because of inefficient absorption and scattering of ultraviolet (UV) radiation (i.e. weak radiation pressure). We examine $\mathcal{D} = 10^{-4}\text{--}10^{-2}$ (corresponding to $\sim 0.01\text{--}1$ times the Galactic dust-to-gas ratio).

3 RESULTS

In this section, we examine the grain motion, focusing on the effects of the parameters in Section 2.7. In the following subsections, we move only one parameter with the others fixed to the fiducial values shown in Table 1. We neglect the time difference between the halo virialization and the ongoing star formation activity; therefore, we regard the formation redshift as the same as the observed redshift (i.e. $z \approx z_{\text{vir}}$). This could be justified because the duration of star formation ($t_{\star} \leq 10^8$ yr) is significantly shorter than the cosmic age (equation A4 in Appendix A).

Before we start moving each parameter, we set the ionization degree f_{ion} and the gas temperature T , which are important for grain charging and gas drag. Determining f_{ion} and T requires a treatment of internal/external ionizing radiation, shock ionization, etc., and is beyond the scope of this paper. To keep our formulation simple (and to avoid additional complexity arising from the detailed physical states of the gas), we basically fix f_{ion} and T by introducing some simple assumptions given below. We expect that $f_{\text{ion}} \approx 1$ at high ζ because of collisional ionization by the halo gas and/or ionizing radiation from nearby galaxies. In contrast, $f_{\text{ion}} \sim 0$ at low ζ in the star-forming disc (assuming that H II regions is confined in small regions). Therefore, we expect that f_{ion} varies from zero in the disc, an intermediate value around the disc–halo interface, and 1 in the halo.

In Fig. 1, we show the grain velocity v_{ζ} as a function of ζ for two different settings regarding f_{ion} . We adopt the fiducial values for the parameters (Table 1). First, we examine the case where $f_{\text{ion}} = 0$ for all ζ . In this case, the drag force is only contributed from direct collisions ($F_{\text{drag}} = F_{\text{drag,direct}}$) regardless of the grain charge. Second, we examine the case where $f_{\text{ion}} = 1$ for all ζ . As mentioned above, this is justified at large ζ . In the upper part ($\zeta \gg H_{\text{d0}}$), grains are charged positively. On the other hand, we obtain $Z_{\text{d}} < 0$ for $f_{\text{ion}} = 1$ in the dense part of the disc. However, it is unlikely that the gas in the disc is all ionized because of its high density ($n_{\text{H}} \gtrsim 100 \text{ cm}^{-3}$); rather, the major part of the disc should be maintained neutral for star formation to continue. Since we do not treat the detailed physical conditions in the disc, we simply neglect Coulomb drag if we obtain $Z_{\text{d}} < 0$, which is equivalent to the assumption that the disc is filled with neutral gas. For the temperature, because of the efficient cooling in the disc, it is expected that T is lower than 10^4 K. We assume $T = 10^4$ K in all regions and discuss the case with a lower temperature later.

The two cases discussed in the above paragraph for $f_{\text{ion}} = 0$ and 1 (and presented in Fig. 1) show the same results at $\zeta \lesssim 20$ pc, since $F_{\text{drag}} = F_{\text{drag,direct}}$ in both cases. In the second case with $f_{\text{ion}} = 1$, since the electron density drops, the grain is positively charged by the photoelectric effect at $\zeta \gtrsim 20$ pc. The positive charge raises gas drag and suppresses the grain velocity at $\zeta \sim 20$ –40 pc. As a consequence, the grain velocity is much lower in the positively charged case than in the zero charge case. At $\zeta \gtrsim 40$ pc, because the ion density drops further, the grain obtains a large velocity.

In the above, we assumed that $T = 10^4$ K, but the temperature may be lower at low ζ . If the temperature is lower, gas drag is weaker. In other words, the case with $T_{\text{gas}} = 10^4$ K gives the strongest drag (the most conservative estimate

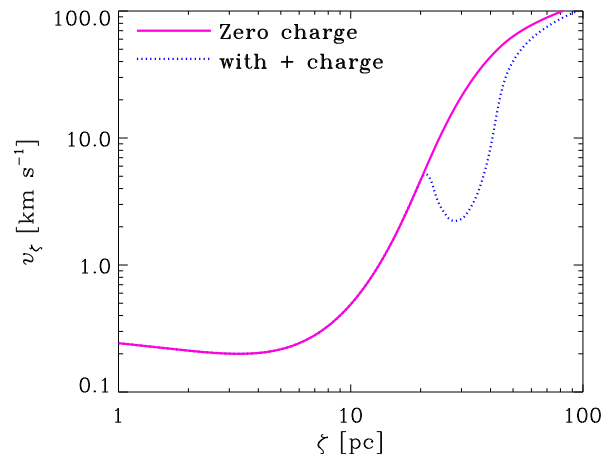


Figure 1. Grain velocity v_{ζ} as a function of ζ for the two test cases regarding the grain charge. The solid line shows the case where $f_{\text{ion}} = 0$. The dotted line presents the case with $f_{\text{ion}} = 1$. In this case, if the resulting grain charge is positive ($Z_{\text{d}} > 0$), we use this grain charge; otherwise, we assume that $Z_{\text{d}} = 0$ (this prescription is correct as long as the gas in the dense part of the disc is neutral).

for the grain escape from the disc) as long as we assume the galactic disc to be composed of neutral gas. In contrast, the upper part of the disc could be ionized (like our Galaxy halo). Since Coulomb drag dominates the total drag force, the gas temperature is not important in the ionized case.

In summary, the second case with $T = 10^4$ K (the dotted line in Fig. 1) gives a conservative estimate of the grain velocity at both low and high ζ . Therefore, we adopt the second case; that is, we assume that $f_{\text{ion}} = 1$ but we neglect negative charging, which could occur at low ζ (or assume that the disc is neutral in such a region).

3.1 Effect of grain properties

First, we show the dependence on the grain radius. In Fig. 2a, we present the grain velocity v_{ζ} as a function of ζ for $a = 1, 0.3, 0.1, 0.03,$ and $0.01 \mu\text{m}$. We observe that the velocity is suppressed to a low level as $v_{\zeta} \sim 0.1 \text{ km s}^{-1}$ at $\zeta \lesssim 10$ pc. The largest dust grain with $a = 1 \mu\text{m}$ once launched is decelerated since gravity becomes dominant over radiation pressure (recall that gravity scales as $\propto a^3$ while the radiation pressure increases roughly as $\propto a^2$ for $a \gtrsim 0.1 \mu\text{m}$). The grain velocity for $a = 0.01 \mu\text{m}$ is low at low ζ because it does not absorb or scatter the stellar light efficiently (i.e. the efficiency of receiving radiation pressure is low). As mentioned above, because of the grain charge, the grain velocity is suppressed at $\zeta \sim 30$ pc, although the gas density drops (see Fig. 2b for the gas profile). The kink structure for $a = 0.03$ and $0.01 \mu\text{m}$ at $\zeta \sim 40$ pc corresponds to the sudden transition from the disc density profile to the halo density. In this sense, we could regard $\zeta \sim 40$ pc as the disc–halo interface. At $\zeta \gtrsim 30$ pc, the grain is accelerated by radiation pressure especially in the cases of $a = 0.1$ and $0.03 \mu\text{m}$. In the case of $a = 0.01 \mu\text{m}$, the velocity approaches the terminal velocity determined by the balance between gas drag and radiation pressure.

We also find that the grain velocity is broadly described

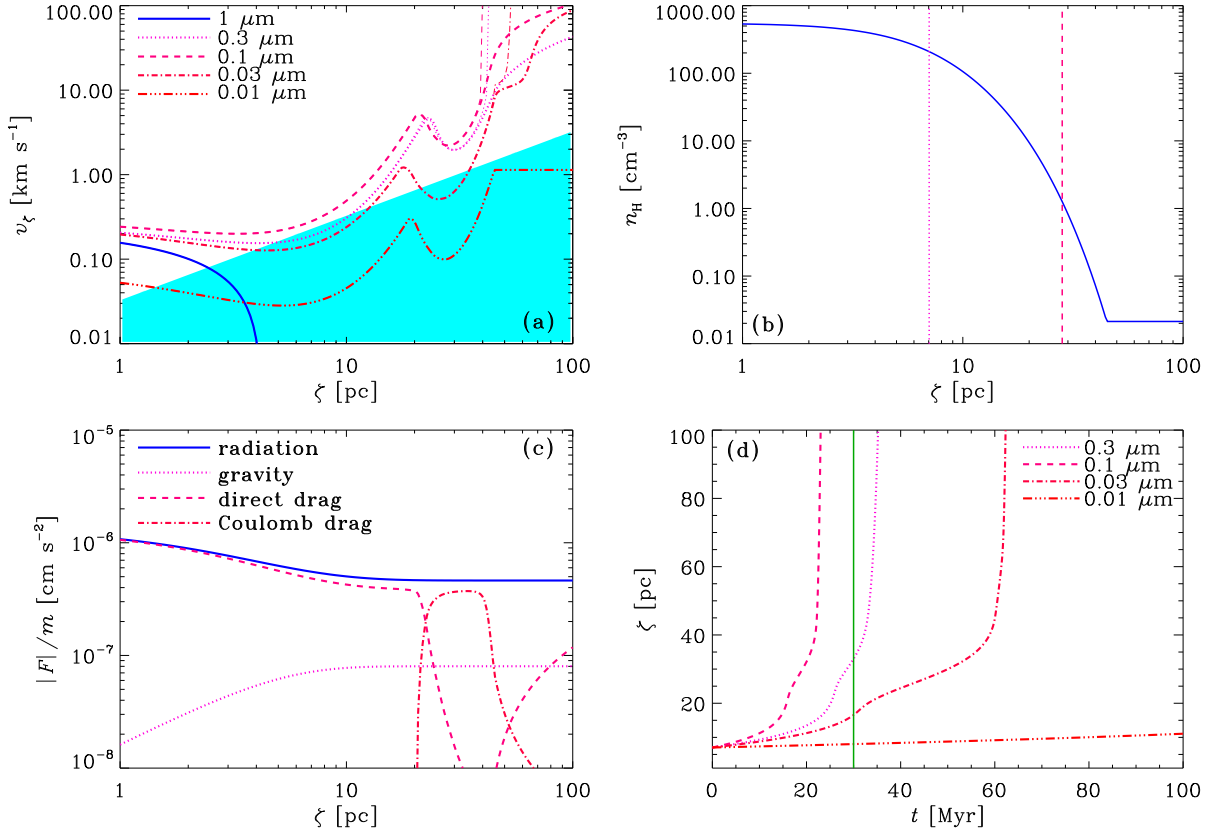


Figure 2. (a) Grain velocity v_ζ as a function of ζ for various grain radii. The thick solid, dotted, dashed, dot-dashed, and triple-dot-dashed lines show the results for $a = 1, 0.3, 0.1, 0.03,$ and $0.01 \mu\text{m}$, respectively. The thin lines, which are almost overlapped with the thick lines, show the equilibrium velocities (the difference between the thick and thin lines is seen only at $\zeta \gtrsim 40$ pc for $a = 0.03\text{--}0.3 \mu\text{m}$). The shaded region shows $v_\zeta < \zeta/t_\star$, which means that the grains are effectively trapped in t_\star (duration of the star formation activity). (b) Gas profile (hydrogen number density as a function of ζ). The vertical dotted line shows the exponential height, where the density drops to the $1/e$ of the central value ($\zeta = 7.0$ pc in this case). The dashed vertical line presents the height at the local velocity minimum of the $a = 0.1 \mu\text{m}$ grain (due to the trapping by the Coulomb drag; $\zeta = 28$ pc in this case; see Panel a). (c) Contribution from the various forces to the acceleration for $a = 0.1 \mu\text{m}$. The solid, dotted, dashed, and dot-dashed lines represent the contribution from radiation force, gravity, drag from direct collisions, and Coulomb drag, respectively. The absolute values are shown. Note that only radiation force is in the positive direction while the other forces are in the negative direction. (d) Grain position ζ as a function of time t for various grain radii with the same line species as in Panel (a). The position of the grain at $t = 0$ is at the exponential height (7.0 pc in this case). The case of $a = 1 \mu\text{m}$ is not shown here. The vertical line shows $t = t_\star$.

by the equilibrium value at each position. The equilibrium velocity is determined by the solution of $dv_\zeta/dt = 0$ in equation (31). In Fig. 2a, we observe that the equilibrium velocity is indistinguishable from the actual velocity except for the cases of $a = 0.03\text{--}0.3 \mu\text{m}$ at $\zeta \gtrsim 40$ pc. Therefore, the grain velocity is determined by the local condition for most of the regions where $v_\zeta \lesssim 10$ km s⁻¹. This is more clearly shown by the individual force components in Fig. 2c (for $a = 0.1 \mu\text{m}$). At $\zeta \lesssim 20$ pc, radiation force is almost equal to drag from direct collisions, while at $\zeta \sim 20\text{--}40$ pc, Coulomb drag is balanced with radiation force. Gravity is always subdominant for the escaping grain. Therefore, the grain motion at $\zeta \lesssim 40$ pc is determined by the balance between radiation force and drag (or in other words, the velocity is adjusted to achieve this balance). At $\zeta \gtrsim 40$ pc, the grain is predominantly accelerated by the radiation force. The drag force also increases at $\zeta \gtrsim 40$ pc because of the increase in grain velocity (note that the density is constant at such a high ζ ; Fig. 2b).

To clarify if the grains are successfully transported outwards within a reasonable time, we show the ‘trapped’ region, which is defined as $\zeta/v_\zeta > t_\star$. The trapped region indicates that the crossing time-scale is longer than the stellar age after which the radiation pressure stops acting on the dust grain. If the major part of the trajectory of a grain in the $v_\zeta\text{--}\zeta$ space passes through the trapped region, the grain is effectively trapped by drag force (or the grain cannot escape within a reasonable time).

We directly show the grain trajectory in the $\zeta\text{--}t$ space in Fig. 2d. We focus on a grain whose initial position is at the exponential height ($\zeta = 7.0$ pc in this case). If we trace a dust grain at the disc plane, it spends most of its time in the disc; thus, we expect that most grains escaping to the halo are located at the upper ($\zeta \sim H_{g0}$) area of the disc. Indeed, if we start from $\zeta = 0$, the grain escape takes ~ 50 Myr for the fiducial parameters. Although the time is still comparable to t_\star , this indicates that grain escape from the mid-plane of the disc may be difficult. Thus, we ‘relax’ the condition and

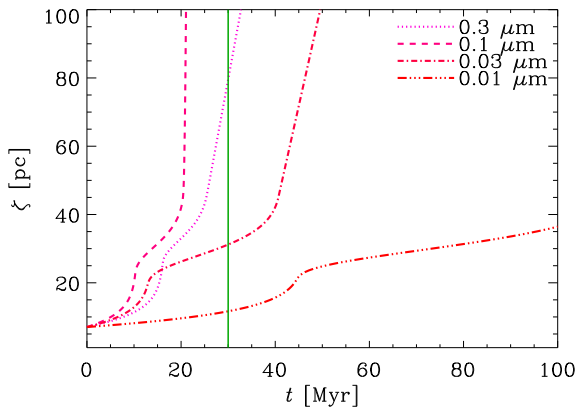


Figure 3. Same as Fig. 2d but for graphite.

start from the exponential height to concentrate on the grain escape from the upper disc (but still in the dense part). Here, the initial velocity is not important since, as shown above, the grain velocity is determined by the local condition in the disc. We observe in Fig. 2d that grains with $a \sim 0.1 \mu\text{m}$ are quickly transported far above the galactic disc, while the ‘trapped’ grains above (grains larger than $0.3 \mu\text{m}$ or smaller than $0.03 \mu\text{m}$) are not efficiently pushed toward high ζ within t_\star . Only in the case of $a = 0.1 \mu\text{m}$ is the grain transported to the halo in $t_\star = 30$ Myr. Other grains spend most of the time around $\zeta \sim 20$ pc where the grains are affected by the strong Coulomb drag.

The radiation force may depend on the grain material. As pointed out by Barsella et al. (1989), graphite grains receive more radiation pressure than silicates; thus, graphite may escape from the disc more easily than silicate. On the other hand, as argued by Bianchi & Ferrara (2005), graphite grains are charged more easily, so that they are more trapped by gas (Coulomb) drag. To investigate the grain material dependence, we show the grain trajectories for graphite in Fig. 3, which is to be compared with Fig. 2d. Because graphite is more efficiently pushed by stellar radiation than silicate, it is more quickly accelerated at low ζ . As a consequence, the grain with $a = 0.3 \mu\text{m}$ as well as that with $a = 0.1 \mu\text{m}$ is transported to a high latitude for graphite. At the same time, at $\zeta \gtrsim 40$ pc, the inclination of the $0.3 \mu\text{m}$ grain on the ζ - t diagram (i.e. the grain velocity) is lower for graphite than for silicate. This is because of stronger Coulomb drag. This result supports both of the above papers: graphite is easily pushed by radiation pressure in the disc because of high radiation pressure, while its velocity could be suppressed around the disc-halo interface by Coulomb drag. Overall, however, the grain trajectory is not drastically different between silicate and graphite, so that we argue that the condition of grain escape is not sensitive to the grain material.

To summarize the above results, grains with $a \sim 0.1 \mu\text{m}$ successfully escape out of the disc even if we consider strong Coulomb drag in the upper disc. Large ($a \gtrsim 1 \mu\text{m}$) grains are captured by gravity, while small ($a \lesssim 0.03 \mu\text{m}$) grains are trapped by gas drag. Comparing silicate and graphite, there is a slight tendency that graphite is less trapped by gas drag in the disc while its velocity is suppressed by Coulomb drag at the disc-halo interface. Overall, the condition for grain escape is not sensitive to the grain species. Below,

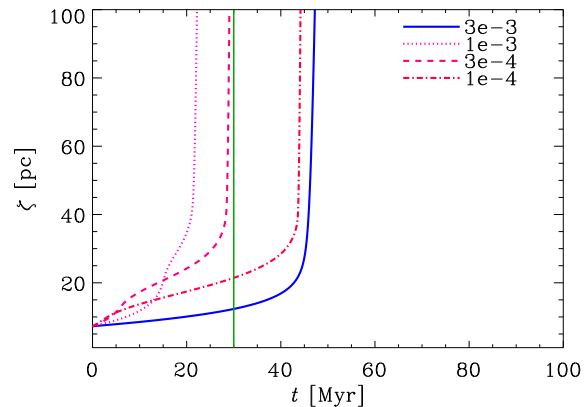


Figure 4. Same as Fig. 2d, but for various dust-to-gas ratios with $a = 0.1 \mu\text{m}$. The solid, dotted, dashed, and dot-dashed lines show the results for $\mathcal{D} = 3 \times 10^{-3}$, 10^{-3} , 3×10^{-4} , and 10^{-4} , respectively.

we concentrate on a silicate grain with $a = 0.1 \mu\text{m}$ unless otherwise stated.

3.2 Effect of dust-to-gas ratio

The dust abundance (dust-to-gas ratio, \mathcal{D}) affects the radiation pressure through the extinction. In Fig. 4, we show the time evolution of the grain position. We do not show the case of $\mathcal{D} = 0.01$, where the dust velocity is negative at $\zeta > 7.3$ pc because of too strong extinction (too weak radiation pressure). On the other hand, if the dust-to-gas ratio is $\lesssim 3 \times 10^{-4}$, it takes more time for the dust grains to reach a high altitude. This is due to the increased grain charge in the low-extinction cases (i.e. grains are more trapped at $\zeta \sim 20$ pc). Therefore, there is an ‘optimum’ dust-to-gas ratio $\mathcal{D} \sim 10^{-3}$, where the stellar light is moderately extinguished to suppress the enhancement of gas drag by grain charging but still radiation pressure is strong enough.

The optimum dust-to-gas ratio is characterized by the dust extinction optical depth. Since we are interested in young stellar population, the major stellar radiation energy absorbed by dust is at UV wavelengths, typically $\sim 0.2 \mu\text{m}$ (Buat & Xu 1996). The dust opacity at $0.2 \mu\text{m}$ in our model is $\kappa_{\text{g,abs}} \sim 1.1 \times 10^4 \mathcal{D} \text{ cm}^2 \text{ g}^{-1}$. The optical depth at $0.2 \mu\text{m}$ is estimated as $\kappa_{\text{g,abs}} \Sigma_{\text{gas}} \approx 8.3 \times 10^2 \mathcal{D} (1 - \epsilon_\star) f_{\text{disc}} (M_{\text{vir}}/10^{10} M_\odot)^{1/3} [(1 + z_{\text{vir}})/11]^2$. Thus, in the fiducial case ($f_{\text{disc}} = 0.5$ and $\epsilon_\star = 0.3$), the opacity is estimated as $\sim 2.9 \times 10^2 \mathcal{D}$. Accordingly, if the dust-to-gas ratio is higher than 3×10^{-3} , the extinction significantly reduces the UV light. This explains the inefficient radiation force for such a large dust-to-gas ratio. For the photoelectric effect, photons at shorter wavelengths (such as $\sim 0.1 \mu\text{m}$) are important; the opacity is higher by a factor of ~ 5 at such a short wavelength. This means that even if $\mathcal{D} = 10^{-3}$, the optical depth for photons causing photoelectric emission becomes of order unity. Thus, Coulomb drag is significantly suppressed if $\mathcal{D} \gtrsim 10^{-3}$. From the above estimates, we can confirm that $\mathcal{D} \sim 10^{-3}$ is the optimum dust-to-gas ratio for grain escape (i.e. strong enough radiation pressure and suppressed photoelectric charging).

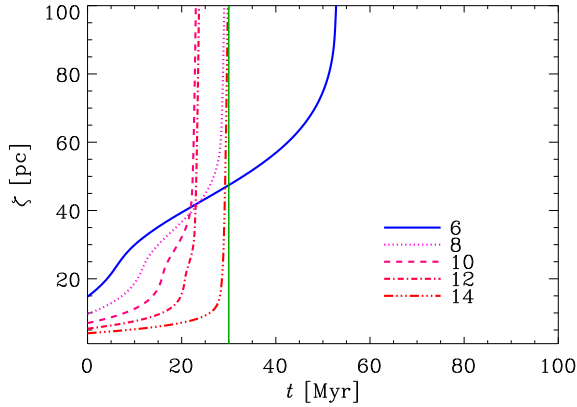


Figure 5. Same as Fig. 2d but for various redshifts with $a = 0.1 \mu\text{m}$. The solid, dotted, dashed, dot-dashed, and triple-dot-dashed lines show the results for $z_{\text{vir}} = 6, 8, 10, 12,$ and 14 , respectively.

3.3 Effect of galaxy parameters

Here we examine the parameters characterizing the galaxy. First, we focus on the effect of formation redshift (z_{vir}). In Fig. 5, we show ζ as a function of t for various z_{vir} . We observe that the dust successfully escapes within $t_{\star} = 30$ Myr if $z_{\text{vir}} \gtrsim 8$. For galaxies with higher z_{vir} , the gas is less extended because of their lower scale height; moreover, the grain velocity at low ζ is not sensitive to z_{vir} because both drag and radiation pressure scale with the surface density (i.e. their scalings with z_{vir} are common). Thus, grain escape occurs on a shorter time-scale for higher z_{vir} . Note that the initial position is the exponential height, which depends on z_{vir} (as well as on M_{vir}). At high ζ , higher- z_{vir} cases have higher grain velocities because of higher stellar surface densities (i.e. higher radiation pressure) for a fixed M_{vir} . For $z_{\text{vir}} = 6$, the grain velocity is kept low; thus, unless the star formation activity lasts much longer than 30 Myr, grains do not escape from the galactic disc. This means that high redshift such as $z \gtrsim 8$ is suitable for grain escape.

Next, we show the dependence on M_{vir} in Fig. 6. There is a broad tendency that dust is more easily accelerated in higher- M_{vir} objects in spite of their stronger gravity (equation 6). Note that grain velocities at low ζ are not sensitive to M_{vir} because both gas density (drag) and stellar surface density (radiation pressure) are scaled in the same way in terms of M_{vir} . However, the gas extension toward the ζ direction (i.e. scale height) is smaller in more massive galaxies. Therefore, it is easier for dust grains to escape from dense regions in more massive objects. However, for $M_{\text{vir}} = 10^{12} M_{\odot}$, the grain escape takes more time: this is because dust extinction is higher (UV is weaker) because of higher column density. As estimated in Section 3.2, the dust optical depth scales as $\propto M_{\text{vir}}^{1/3}$. This means that the dust opacity for $M_{\text{vir}} = 10^{12} M_{\odot}$ is $10^{2/3} \approx 4.6$ times higher than that for $M_{\text{vir}} = 10^{10} M_{\odot}$. Indeed, if we suppress the dust-to-gas ratio by a factor 4.6 (~ 0.002), the dust grain successfully escapes from the disc within $t_{\star} = 30$ Myr. However, it may not be easy to maintain such massive objects dust-poor (1/50 times the solar), since they are located in high-density peaks in the Universe (see also Section 4.1). To summarize, with a fixed dust-to-gas

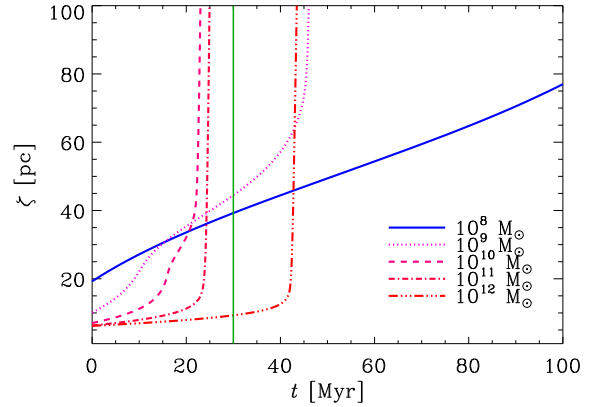


Figure 6. Same as Fig. 2d but for various virial masses with $a = 0.1 \mu\text{m}$. The solid, dotted, dashed, dot-dashed, and triple-dot-dashed lines show the results for $M_{\text{vir}} = 10^8, 10^9, 10^{10}, 10^{11}$ and $10^{12} M_{\odot}$, respectively.

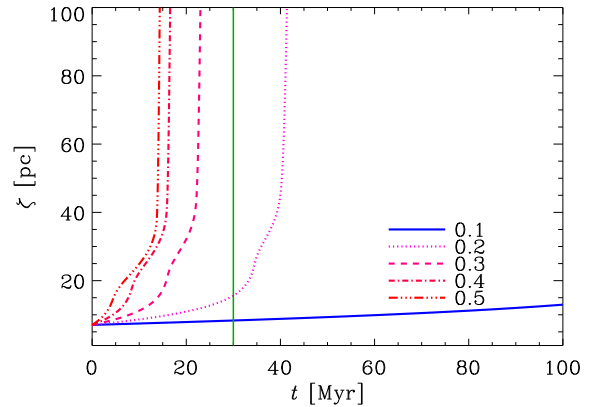


Figure 7. Same as Fig. 4 but for various star formation efficiencies with $a = 0.1 \mu\text{m}$. The solid, dotted, dashed, dot-dashed, and triple-dot-dashed lines show the results for $\epsilon_{\star} = 0.1, 0.2, 0.3, 0.4,$ and 0.5 , respectively.

ratio, a high mass does not necessarily mean a more dust escape from the disc. For low-mass ($M_{\text{vir}} \lesssim 10^9 M_{\odot}$) objects, grains are less efficiently accelerated because the gas is more extended (i.e. for the same reason as in the case of low $z_{\text{vir}} \sim 6$). Therefore, massive galaxies with $M_{\text{vir}} \gtrsim 10^{10} M_{\odot}$ are favourable for grain escape; but extremely dust-poor ($\sim 1/50$ times the Milky Way dust-to-gas ratio) condition is required for very massive ($M_{\text{vir}} \sim 10^{12} M_{\odot}$) objects.

We examine the dependence on the star formation efficiency ϵ_{\star} in Fig. 7. As expected, grains are more efficiently accelerated in the case of higher ϵ_{\star} because of higher radiation pressure. In the case of $\epsilon_{\star} \leq 0.2$, the grain does not reach a high $\zeta \gtrsim 40$ pc within $t_{\star} = 30$ Myr. Thus, a high star formation efficiency $\epsilon_{\star} \gtrsim 0.3$ (or $\epsilon_{\star} f_{\text{disc}} \gtrsim 0.15$ for the total conversion efficiency of baryon into stars) is necessary for grain escape.

In Fig. 8, we show the ζ - t relation for different stellar ages t_{\star} and different grain radii. We observe that the outward motion tends to be slower for older stellar ages. Note that we fixed the total stellar mass formed (thus, a larger t_{\star}

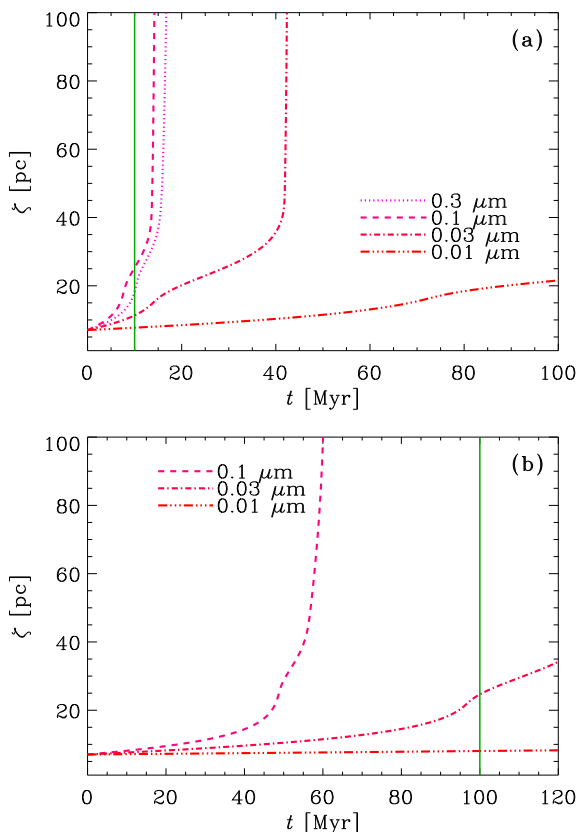


Figure 8. Same as Fig. 2d but for different stellar ages, $t_\star = 10$ and 100 Myr for panels (a) and (b), respectively. The different lines show different grain radii with the same line species as in Fig. 2d (also shown in the legend). Note that we do not show $a = 1 \mu\text{m}$ ($a = 1$ and $0.3 \mu\text{m}$) in panel (a) [panel(b)] because the grain velocity becomes negative.

means lower star formation rate, i.e. lower UV luminosity). Grains with $a \sim 0.1 \mu\text{m}$ are pushed efficiently by radiation pressure and escape from the disc within t_\star for $t_\star = 100$ Myr. In contrast, in the case of $t_\star = 10$ Myr, the grain is difficult to escape within the short age. Thus, we conclude that sustaining star formation activity for a long ($\gtrsim 30$ Myr) time is necessary to push the dust grains continuously out of the galactic disc.

4 DISCUSSION

4.1 Condition for grain escape

We have shown that only grains with $a \sim 0.1 \mu\text{m}$ can be transported to the halo. Smaller ($a \lesssim 0.03 \mu\text{m}$) and larger ($a \gtrsim 1 \mu\text{m}$) grains are efficiently trapped in the galactic disc or at disc–halo interface because of gas drag and gravity, respectively. Graphite is more efficiently pushed by radiation pressure at low ζ than silicate, while it is less efficiently accelerated in the halo. We have also found that there is an optimum dust-to-gas ratio, $\mathcal{D} \sim 10^{-3}$, for grain escape. Galaxies with $z_{\text{vir}} \gtrsim 8$ are efficient in pushing dust out of the disc. There is also an optimum virial mass range for grain escape, $M_{\text{vir}} \sim 10^{10}–10^{11} M_\odot$. In order to achieve a sufficient

stellar brightness for grain escape, more than 15 per cent of the baryon should be converted to the stars in the current star formation episode, and the star formation should continuously last longer than ~ 30 Myr. These conditions can be used to model the dust supply to galaxy halos at high redshift in an extended framework such as a semi-analytic model.

We have found that the optimum dust-to-gas ratio is determined by the optical depth at UV wavelengths. If the dust-to-gas ratio is too high, the stellar UV light is heavily extinguished so that radiation pressure becomes too weak to push the grain. The condition for the weak extinction is determined by the optical depth < 1 at a typical UV wavelength for stellar radiation ($\sim 0.2 \mu\text{m}$). The optical depth at $0.2 \mu\text{m}$ is estimated as $\tau_{0.2} \sim 8.3 \times 10^2 \mathcal{D} (1 - \epsilon_\star) f_{\text{disc}} (M_{\text{vir}}/10^{10} M_\odot)^{1/3} [(1 + z_{\text{vir}})/11]^2$ (Section 3.2). If this is smaller than 1, the extinction effect is not significant. If the dust-to-gas ratio is too low, stellar UV emission is not attenuated, so that it efficiently charges grain positively. This enhances Coulomb drag, and suppresses the grain velocities. Thus, it is desirable that the optical depth at a typical wavelength of the photoelectric effect ($\sim 0.1 \mu\text{m}$) is larger than 1 (corresponding optical depth at $\sim 0.2 \mu\text{m}$ is roughly 1/5). Therefore, the optimum dust-to-gas ratio, denoted as $\mathcal{D}_{\text{optimum}}$, is determined by the condition $0.2 < \tau_{0.2} < 1$. This is translated into the following condition:

$$\mathcal{D}_{\text{optimum}} \sim (0.6-3) \times 10^{-3} \left(\frac{1 - \epsilon_\star}{0.7} \right)^{-1} \left(\frac{f_{\text{disc}}}{0.5} \right)^{-1} \left(\frac{M_{\text{vir}}}{10^{10} M_\odot} \right)^{-1/3} \times \left(\frac{1 + z_{\text{vir}}}{11} \right)^{-2}. \quad (32)$$

Thus, the optimum dust-to-gas ratio is roughly $\mathcal{D}_{\text{eff}} \sim 10^{-3}$ in the fiducial condition, but the above formula can be used for other parameter values.

For $M_{\text{vir}} = 10^{10}–10^{11} M_\odot$, the corresponding stellar mass with $f_{\text{disc}} = 0.5$ and $\epsilon_\star = 0.3$ is $2 \times 10^8–2 \times 10^9 M_\odot$. According to a semi-analytic model by Popping et al. (2017), the typical dust-to-gas ratio in the above stellar mass range is $\sim 3 \times 10^{-5}–3 \times 10^{-3}$ at $z \gtrsim 7$, overlapping with the above optimum dust-to-gas ratio. However, for $M_{\text{vir}} = 10^{12} M_\odot$, the optimum dust-to-gas ratio is $\lesssim 10^{-4}$, but it is difficult to maintain the dust-to-gas ratio of such a massive galaxy lower than 10^{-4} (Popping et al. 2017). The above dust-to-gas ratio would indicate a metallicity of $1/100 Z_\odot$ if we assume a proportionality between dust-to-gas ratio and metallicity, and a theoretical stellar-mass–metallicity relation at $z \sim 10$ indicates that a galaxy with the above stellar mass range has a higher metallicity (Torrey et al. 2019).

4.2 Dynamical effects of radiation pressure

The grain motion have different characteristic behaviours at different heights from the disc plane. At low $\zeta \ll H_{\text{g0}}$, grains have typically $v_\zeta \sim 0.1 \text{ km s}^{-1}$ unless the grain radius is as large as $\sim 1 \mu\text{m}$ (Fig. 2a). This means that the radiation pressure causes dust–gas decoupling on a vertical scale of $\sim v_\zeta t_\star \sim 3.1(v_\zeta/0.1 \text{ km s}^{-1})(t_\star/30 \text{ Myr}) \text{ pc}$. Thus, it is important to note that radiation pressure produces a ‘drift’ of dust grains relative to the gas on a spatial scale of \sim a few pc. The implication of this is that, if we calculate grain dynamics on scale \lesssim a few pc on a time-scale of a few tens Myr

(\sim a typical duration of a star formation episode), we need to take into account the effect of radiation pressure on the grain motion.

At intermediate $\zeta \sim$ a few $\times H_{g0}$, although the density drops significantly, grain motions are strongly affected by gas drag because of the grain charge. Therefore, even if the gas density drops, the grain velocities stay around 1 km s^{-1} . Larger grains have larger velocities because of their lower surface-to-volume ratio (less drag per grain mass) and larger Q_{rad} . However, if the grains are too large, gravity suppresses the grain velocity. Therefore, there is an optimum grain radius $\sim 0.1 \mu\text{m}$ for grain escape from the disc.

At large $\zeta \gtrsim 10H_{g0}$, grains with $a \sim 0.1 \mu\text{m}$ are rapidly accelerated to $> 10 \text{ km s}^{-1}$. At this stage, gas drag can become so weak that grains are accelerated freely by radiation pressure. Note that, since both gravity and radiation pressure are constant at large ζ in our approximation of an infinitely wide disc, the grains continue to be accelerated outward once they escape from the disc. Thus, if a grain with $a \lesssim 0.1 \mu\text{m}$ somehow reaches $\zeta \sim 10H_{g0}$, it is successfully injected into the halo.

4.3 Observational implications for the grain size in galaxy halos

Hirashita & Lin (2018) showed that galaxy halos at $z \lesssim 2$ contain dust grains with $a \sim 0.01\text{--}0.03 \mu\text{m}$, based on the reddening curves of objects tracing galaxy halos (such as Mg II absorbers; Ménard & Fukugita 2012). According to the results above, the grains with $a \sim 0.01 \mu\text{m}$ do not escape from the galaxy disc, while larger grains with $a \sim 0.1 \mu\text{m}$ can be supplied to the halo. Therefore, the dust transport mechanism by radiation pressure has difficulty in explaining the small grains derived by Hirashita & Lin (2018). We should note that hydrodynamical motion driven by SN feedback (i.e. galactic wind) could also transport dust grains to halos. Hou et al. (2017), using a simulation of single disc galaxy, showed that the grains transported by stellar feedback are biased to large ($> 0.03 \mu\text{m}$) sizes. This is because dust grains formed by SNe have large sizes and they are transported before they are processed in the ISM by shattering. Aoyama et al. (2018) confirmed this conclusion by a cosmological simulation. Therefore, SN feedback does not seem to provide small dust grains to galaxy halos.

Dust may be processed in the CGM or IGM. It may be destroyed by sputtering, which, however, tends to destroy small grains more efficiently than large ones (Draine & Salpeter 1979; Nozawa et al. 2006). Thus, sputtering generally has difficulty in producing a grain size distribution in excess of small grains. Indeed, Bianchi & Ferrara (2005) showed that the grain size distribution after sputtering in the IGM is still flat with a shift to smaller radii. Such a grain size distribution cannot explain the strongly rising trend of the reddening in Mg II absorbers toward short UV wavelengths.

The observational evidence of small grains in the regions out of galaxies is based on Mg II absorbers and the CGM, which could have some density contrast. Lan & Fukugita (2017) proposed that Mg II absorbers are associated with clouds with a gas density of $\sim 0.3 \text{ cm}^{-3}$. This density is high enough for grain–grain collisions to occur on a time-scale of

$\sim 1 \text{ Gyr}$ (Aoyama et al. 2017), which is shorter than the interval between $z \sim 10$, in which our model is interested, and $z \sim 2$, where the Mg II absorbers are sampled. Therefore, the small grains may have been formed by shattering in the circum-galactic environment.

Eventually, we have to combine the above discussions with the evolution of grain size distribution in a galactic disc. The grain size distribution in the early stage of galaxy evolution is biased to large ($a \gtrsim 0.1 \mu\text{m}$) sizes because dust grains produced by stellar sources are considered to be large (e.g. Nozawa et al. 2007; Bianchi & Schneider 2007; Yasuda & Kozasa 2012; Dell’Agli et al. 2017). Therefore, we expect that grains with $a \sim 0.1 \mu\text{m}$ exist even in the early phase of galaxy evolution. On the other hand, we have shown in Section 3.2 that the optimum dust-to-gas ratio for grain escape is $\mathcal{D} \sim 10^{-3}$, which is much less than the dust-to-gas ratio in solar-metallicity environments ($\mathcal{D} \sim 10^{-2}$). If we assume a rough proportionality between dust-to-gas ratio and metallicity (Z), grain escape occurs most efficiently at $Z \sim 0.1 Z_{\odot}$. It is interesting to note that this metallicity also corresponds to the metallicity level at which the grain size distribution is strongly modified by the interstellar processing (e.g. Asano et al. 2013). Therefore, it is desirable in the future to solve the combined effects between the evolution of grain size distribution in the galactic disc and the dust transport to the halo.

4.4 Implication for observed galaxy populations at high redshift

In Section 3.3, we have shown that the star formation efficiency ϵ_{\star} higher than 0.3 (or the baryonic mass fraction converted to stars $\epsilon_{\star} f_{\text{disc}} \gtrsim 0.15$) is required to efficiently push the dust by radiation pressure. In the previous subsection, we have also argued that star formation needs to last $\gtrsim 30 \text{ Myr}$ to transport the dust to the halo. These numbers enable us to estimate the SFR and stellar mass in galaxies whose halos are enriched with dust.

Our formulation is based on disc geometry, so that the surface density was useful. Here, we need global quantities. The total stellar mass, $M_{\star} = (\pi r_{\text{disc}}^2) \Sigma_{\text{b}}$, is estimated as (see equations 3 and 4)

$$\begin{aligned} M_{\star} &= \epsilon_{\star} (\Omega_{\text{b}}/\Omega_{\text{M}}) f_{\text{disc}} M_{\text{vir}} \\ &= 2.0 \times 10^8 \left(\frac{\epsilon_{\star}}{0.3} \right) \left(\frac{f_{\text{disc}}}{0.5} \right) \left(\frac{M_{\text{vir}}}{10^{10} M_{\odot}} \right) M_{\odot}. \end{aligned} \quad (33)$$

The star formation should last $\gtrsim 30 \text{ Myr}$ for grain escape. This, combined with the above stellar mass, indicates SFR $\lesssim 7(M_{\text{vir}}/10^{10} M_{\odot}) M_{\odot} \text{ yr}^{-1}$. LBGs typically have a comparable or larger mass than the above (e.g. Bouwens et al. 2016). Hashimoto et al. (2018) analyzed the SED of a galaxy at $z = 9.1$, and found that it experienced an old star formation episode, which lasted $\sim 100 \text{ Myr}$ at $z \sim 15\text{--}12$. The established stellar mass by this star formation activity is $\sim 10^9 M_{\odot}$, which is larger than the value estimated in equation (33). Thus, it is expected that this object had sufficiently strong radiation pressure for halo enrichment with dust (with grain radius $\sim 0.1 \mu\text{m}$). If such a galaxy is prevalent at $z \sim 10$, we should consider dust enrichment in galaxy halos by radiation pressure. We need a statistical sample of galaxies at $z \sim 10$ to draw a definite conclusion.

In our one-dimensional framework, it is difficult to predict how much dust is supplied to halos. Nevertheless, the following rough estimate is possible. We consider a halo with $M_{\text{vir}} = 10^{10} M_{\odot}$. With $f_{\text{disc}} = 0.5$, the gas mass in the halo is estimated as $6.7 \times 10^8 M_{\odot}$, and that in the disc as the same amount. We have shown that dust grains with $a \sim 0.1 \mu\text{m}$ escape from the galactic disc. Grains with $a \sim 0.3 \mu\text{m}$ could marginally escape (Figs. 2d and 3). Adopting an MRN grain size distribution ($\propto a^{-3.5}$) with lower and upper grain radii being $0.005 \mu\text{m}$ and $0.25 \mu\text{m}$, respectively, we estimate that the mass fraction of dust with $a \geq 0.1 \mu\text{m}$ is 0.43. As shown above, the dust-to-gas ratio at which the radiation pressure works the most efficiently is $\mathcal{D} \sim 10^{-3}$ (Section 3.2). If we assume a star formation efficiency of 0.3, the remaining gas mass in the disc is $4.7 \times 10^8 M_{\odot}$, which indicates that the total dust mass is $\sim 4.7 \times 10^5 M_{\odot}$ with $\mathcal{D} = 10^{-3}$. Therefore, the dust mass transported to the halo is expected to be $\sim 2.0 \times 10^5 M_{\odot}$. The total stellar mass, on the other hand, is $2.0 \times 10^8 M_{\odot}$. Thus, the mass ratio of the halo dust to the stars is $\sim 10^{-3}$. From an observational point of view, Hirashita & Lin (2018), based on Ménard et al. (2010), argued that the observed mass ratio of the halo dust to the stars is $\sim 10^{-3}$ for low-redshift galaxies. Comparing the numbers, high-redshift halos could be as dust-rich as low-redshift halos. Therefore, dust transport by radiation pressure in high-redshift galaxies should be considered to understand the origin of the dust in halos.

If grains with $a \sim 0.1 \mu\text{m}$ efficiently escape out of the galactic disc, this could have a significant influence on the dust evolution in the galactic disc. First, the dust abundance in the galactic disc could be decreased or the dust distribution is extended toward the galaxy halo. Such an extended dust component will have a lower temperature than that in the disc, because it is farther from the radiation sources (i.e. stars in the disc). Since lower-temperature dust emits less radiation, extended dust distribution could be a reason for non-detection of dust in a large fraction of high-redshift ($z \gtrsim 7$) galaxies by ALMA. Second, the remaining dust in the galactic disc could be biased to small ($a \lesssim 0.03 \mu\text{m}$) grains because large ($a \sim 0.1 \mu\text{m}$) grains are preferentially transported out of the disc. This could produce a steep extinction curve. Indeed, as shown by Hashimoto et al. (2019), those galaxies at $z > 6.5$ whose dust emission is not detected by ALMA tend to have steeper extinction curves, if their positions in the so-called IRX- β diagram are interpreted as reflecting the extinction (attenuation) curve. Selective loss of relatively large ($a \sim 0.1 \mu\text{m}$) grains could explain this tendency.

4.5 Uncertainties

We simplified the problem to make it analytically tractable. It is worth mentioning the limitations and uncertainties caused by some simplifications.

The initial velocity and position are not important as long as it is set at $\zeta \lesssim 20$ pc (several scale heights), since the grain velocity is determined by the equilibrium value mainly determined by the balance between gas drag and radiation pressure (Section 3.1; Fig. 2a). For example, the typical drag time-scale in the galactic disc is $\sim 10^3$ yr; thus, even if the initial grain velocity is 1000 km s^{-1} , the grain only moves 1 pc. This means that the grains are efficiently decelerated by

gas drag on a scale much smaller than the disc scale height. Therefore, our results are robust against the initial velocity. In contrast, the initial velocity is important if the initial position is above several scale heights.

The vertical gas structure is determined by the gravity which is characterized by β and H_{M} . These parameters are scaled with M_{vir} and z_{vir} (equations 6 and 7). These scalings and the associated normalizing factors might be too simple. However, the relative strength between gas drag and radiation pressure is rather robust because both scale with the surface densities of the galactic disc. As long as we fix the star formation efficiency, thus, the relative strength between gas drag and radiation pressure, which broadly determines the condition for grain escape, is not sensitive to the assumed scalings. For the same reason, the condition for grain escape is not sensitive to the change of q_{disc} .

The scale height is also governed by the velocity dispersion of the gas, σ . The change of σ does not affect our conclusions. If we assume a smaller σ , the gas density becomes σ^2 times larger, so that the velocity is suppressed roughly by a factor of σ^2 . However, the disc is also $1/\sigma^2$ times thinner. Therefore, the time-scale of grain escape from the disc is not sensitive to σ .

If the grains are charged and magnetic field is present, the grain motion is also affected by the Lorentz force. However, it is not clear yet whether magnetic fields are amplified efficiently in high-redshift galaxies. The role of magnetic field is to constrain the motion of charged grains to the direction of magnetic field. Therefore, as long as the magnetic field has a significant poloidal component (or a component open to the ζ direction), the grain escape condition is not significantly affected so that the results obtained in this paper is still applicable for the grain motion in the ζ direction.

As mentioned at the beginning of Section 3, our simple model is not capable of treating inhomogeneity of gas structure in terms of ionization degree and temperature. The metallicity (and dust-to-gas ratio) could also be strongly inhomogeneous (Pallottini et al. 2017). In the future work, it is desirable to solve these features, but it should also be kept in mind that, to this goal, we need to make a comprehensive model of hydrodynamics (including star formation and stellar feedback) and radiation transfer. Our simple models in this paper gives a first guide to such more complicated models, or provides a basis on which we model dust supply from galactic discs to halos in semi-analytic models.

5 CONCLUSION

For the purpose of clarifying the origin of dust in galaxy halos or in the CGM/IGM, we have investigated dust transport from the galactic disc to the halo (‘grain escape’) by radiation pressure in high-redshift galaxies. We have considered radiation pressure arising from the star formation activities and focused on the redshift range where recent observations indicate the occurrence of active star formation ($z \sim 10$). We have solved the motion of a grain with various sizes considering radiation pressure, gas drag, and gravity in the vertical direction of the galactic disc. Radiation pressure is estimated in a consistent manner with the stellar SED and dust extinction.

We give the virial mass M_{vir} and the formation redshift

z_{vir} as parameters. First, we focus on $M_{\text{vir}} = 10^{10} M_{\odot}$ and $z_{\text{vir}} = 10$. We point out that grain charging by UV light plays an important role in gas drag at a few–10 scale heights of the galactic disc and that the grain velocities are suppressed to $\sim 1 \text{ km s}^{-1}$. Graphite grains are slightly easier to escape from the disc than silicates because they receive more radiation force. However, graphite has slightly lower velocity in the halo than silicate because of its larger charge (stronger drag). We find that grains with radius $a \sim 0.1 \mu\text{m}$ successfully escape from the galactic disc if the current star formation episode converts more than 15 per cent of the baryon content into stars and lasts $\gtrsim 30 \text{ Myr}$. Larger ($a \gtrsim 1 \mu\text{m}$) grains are efficiently trapped in the disc because of its large inertia (gravity), while small ($a \lesssim 0.01 \mu\text{m}$) grains are also strongly influenced by gas drag because of their low efficiency of receiving radiation force.

Next we vary M_{vir} and z_{vir} and examine if a grain with $a = 0.1 \mu\text{m}$ could escape from the disc. High-redshift galaxies ($z_{\text{vir}} \gtrsim 8$) are favourable for grain escape because of their lower scale height (i.e. it takes less time to cross the dense region). For the same reason, more massive galaxies are favorable for grain escape; however, we also find that if the galaxy is too massive ($M_{\text{vir}} \gtrsim 10^{12} M_{\odot}$), dust extinction is high enough to extinguish a significant fraction of stellar UV with $\mathcal{D} \sim 10^{-3}$. Maintaining a condition with $\mathcal{D} \ll 10^{-3}$ (or $Z \ll 0.1 Z_{\odot}$) in such a massive object may be difficult. Thus, we argue that there is an optimum range of the virial mass, $M_{\text{vir}} \sim 10^{10}\text{--}10^{11} M_{\odot}$, for grain escape. We estimate that the dust mass in the halos of these galaxies could reach 10^{-3} times the stellar mass in the disc, which is comparable to the dust abundance found in the CGM at $z \lesssim 3$. A recently found galaxy at $z = 9.1$ (Hashimoto et al. 2018) satisfies the condition of grain escape for $a \sim 0.1 \mu\text{m}$, implying that dust injection to halo by radiation pressure already occurred at $z \sim 10$. Therefore, we conclude that radiation pressure in high- z galaxies is important in considering the origin of dust in galaxy halos.

ACKNOWLEDGEMENTS

We are grateful to W.-H. Shao, A. Ferrara, and M. Murgia for useful discussions and to the anonymous referee for helpful comments. HH thanks the Ministry of Science and Technology for support through grant MOST 105-2112-M-001-027-MY3 and MOST 107-2923-M-001-003-MY3 (RFBR 18-52-52-006). This work was supported by NAOJ ALMA Scientific Research Grant Number 2016-01A.

REFERENCES

- Aguirre A. N., 1999, *ApJ*, **512**, L19
- Akimkin V. V., Kirsanova M. S., Pavlyuchenkov Y. N., Wiebe D. S., 2015, *MNRAS*, **449**, 440
- Akimkin V. V., Kirsanova M. S., Pavlyuchenkov Y. N., Wiebe D. S., 2017, *MNRAS*, **469**, 630
- Aoyama S., Hou K.-C., Shimizu I., Hirashita H., Todoroki K., Choi J.-H., Nagamine K., 2017, *MNRAS*, **466**, 105
- Aoyama S., Hou K.-C., Hirashita H., Nagamine K., Shimizu I., 2018, *MNRAS*, **478**, 4905
- Asano R. S., Takeuchi T. T., Hirashita H., Nozawa T., 2013, *MNRAS*, **432**, 637
- Barnes J., Efstathiou G., 1987, *ApJ*, **319**, 575
- Barsella B., Ferrini F., Greenberg J. M., Aiello S., 1989, *A&A*, **209**, 349
- Bekki K., Hirashita H., Tsujimoto T., 2015, *ApJ*, **810**, 39
- Bianchi S., Ferrara A., 2005, *MNRAS*, **358**, 379
- Bianchi S., Schneider R., 2007, *MNRAS*, **378**, 973
- Bohren C. F., Huffman D. R., 1983, *Absorption and Scattering of Light by Small Particles*. Wiley
- Bouwens R. J., et al., 2016, *ApJ*, **833**, 72
- Bruzual G., Charlot S., 2003, *MNRAS*, **344**, 1000
- Buat V., Xu C., 1996, *A&A*, **306**, 61
- Chabrier G., 2003, *PASP*, **115**, 763
- Ciardi B., Ferrara A., Governato F., Jenkins A., 2000, *MNRAS*, **314**, 611
- Crocker R. M., Krumholz M. R., Thompson T. A., Baumgardt H., Mackey D., 2018, *MNRAS*, **481**, 4895
- Davies J. I., Alton P., Bianchi S., Trewheella M., 1998, *MNRAS*, **300**, 1006
- de Boer H., 1991, in Bloemen H., ed., *IAU Symposium Vol. 144, The Interstellar Disk-Halo Connection in Galaxies*. pp 333–336
- Dell’Agli F., García-Hernández D. A., Schneider R., Ventura P., La Franca F., Valiante R., Marini E., Di Criscienzo M., 2017, *MNRAS*, **467**, 4431
- Draine B. T., 1978, *ApJS*, **36**, 595
- Draine B. T., Salpeter E. E., 1979, *ApJ*, **231**, 77
- Draine B. T., Sutin B., 1987, *ApJ*, **320**, 803
- Ferrara A., 1993, *ApJ*, **407**, 157
- Ferrara A., Ferrini F., Barsella B., Franco J., 1991, *ApJ*, **381**, 137
- Ferrara A., Pettini M., Shchekinov Y., 2000, *MNRAS*, **319**, 539
- Franco J., Ferrini F., Ferrara A., Barsella B., 1991, *ApJ*, **366**, 443
- Furlanetto S. R., Oh S. P., Briggs F. H., 2006, *Phys. Rep.*, **433**, 181
- Hashimoto T., et al., 2018, *Nature*, **557**, 392
- Hashimoto T., et al., 2019, arXiv e-prints,
- Hirashita H., Lin C.-Y., 2018, arXiv e-prints,
- Hou K.-C., Hirashita H., Nagamine K., Aoyama S., Shimizu I., 2017, *MNRAS*, **469**, 870
- Inoue A. K., Kamaya H., 2003, *MNRAS*, **341**, L7
- Inoue A. K., Kamaya H., 2004, *MNRAS*, **350**, 729
- Inoue A. K., Kamaya H., 2010, *Earth, Planets, and Space*, **62**, 69
- Ishiki S., Okamoto T., Inoue A. K., 2018, *MNRAS*, **474**, 1935
- Kereš D., Katz N., Weinberg D. H., Davé R., 2005, *MNRAS*, **363**, 2
- Kitayama T., Suto Y., 1996, *ApJ*, **469**, 480
- Lan T.-W., Fukugita M., 2017, *ApJ*, **850**, 156
- Laporte N., et al., 2017, *ApJ*, **837**, L21
- Masaki S., Yoshida N., 2012, *MNRAS*, **423**, L117
- Mathis J. S., Rumpl W., Nordsieck K. H., 1977, *ApJ*, **217**, 425
- McKee C. F., Hollenbach D. J., Seab G. C., Tielens A. G. G. M., 1987, *ApJ*, **318**, 674
- McKinnon R., Torrey P., Vogelsberger M., 2016, *MNRAS*, **457**, 3775
- McKinnon R., Vogelsberger M., Torrey P., Marinacci F., Kannan R., 2018, *MNRAS*, **478**, 2851
- Ménard B., Fukugita M., 2012, *ApJ*, **754**, 116
- Ménard B., Scranton R., Fukugita M., Richards G., 2010, *MNRAS*, **405**, 1025
- Nakanishi H., Sofue Y., 2016, *PASJ*, **68**, 5
- Nozawa T., Kozasa T., Habe A., 2006, *ApJ*, **648**, 435
- Nozawa T., Kozasa T., Habe A., Dwek E., Umeda H., Tominaga N., Maeda K., Nomoto K., 2007, *ApJ*, **666**, 955
- Pallottini A., Ferrara A., Gallerani S., Vallini L., Maiolino R., Salvadori S., 2017, *MNRAS*, **465**, 2540
- Peebles P. J. E., 1980, *The Large-Scale Structure of the Universe*. Princeton University Press, Princeton
- Peek J. E. G., Ménard B., Corrales L., 2015, *ApJ*, **813**, 7
- Pei Y. C., 1992, *ApJ*, **395**, 130

- Popping G., Somerville R. S., Galametz M., 2017, *MNRAS*, **471**, 3152
- Reed D., Gardner J., Quinn T., Stadel J., Fardal M., Lake G., Governato F., 2003, *MNRAS*, **346**, 565
- Shustov B. M., Vibe D. Z., 1995, *Astronomy Reports*, **39**, 578
- Simonsen J. T., Hannestad S., 1999, *A&A*, **351**, 1
- Spitzer L., 1978, *Physical Processes in the Interstellar Medium*. Wiley, New York
- Tamura Y., et al., 2019, *ApJ*, **874**, 27
- Torrey P., et al., 2019, *MNRAS*,
- Trimble V., 2000, *Milky Way and Galaxies*, 4th edn. Springer, New York
- Veilleux S., Cecil G., Bland-Hawthorn J., 2005, *ARA&A*, **43**, 769
- Watson D., Christensen L., Knudsen K. K., Richard J., Gallazzi A., Michałowski M. J., 2015, *Nature*, **519**, 327
- Weingartner J. C., Draine B. T., 2001a, *ApJS*, **134**, 263
- Weingartner J. C., Draine B. T., 2001b, *ApJ*, **548**, 296
- Weingartner J. C., Draine B. T., 2001c, *ApJ*, **553**, 581
- Yasuda Y., Kozasa T., 2012, *ApJ*, **745**, 159
- Yim K., Wong T., Xue R., Rand R. J., Rosolowsky E., van der Hulst J. M., Benjamin R., Murphy E. J., 2014, *AJ*, **148**, 127
- York D. G., et al., 2000, *AJ*, **120**, 1579
- Young L. M., Lo K. Y., 1997, *ApJ*, **490**, 710
- Zu Y., Weinberg D. H., Davé R., Fardal M., Katz N., Kereš D., Oppenheimer B. D., 2011, *MNRAS*, **412**, 1059

APPENDIX A: RELEVANT QUANTITIES

For convenience, we give numerical estimates of some quantities used in the text.

The virial radius, r_{vir} , is numerically estimated based on equation (2) as

$$r_{\text{vir}} = 6.0 \left(\frac{M_{\text{vir}}}{10^{10} M_{\odot}} \right)^{1/3} \left(\frac{1+z_{\text{vir}}}{11} \right)^{-1} \text{ kpc.} \quad (\text{A1})$$

The disc radius is accordingly

$$r_{\text{disc}} = 1.1 \left(\frac{q_{\text{disc}}}{0.18} \right) \left(\frac{M_{\text{vir}}}{10^{10} M_{\odot}} \right)^{1/3} \left(\frac{1+z_{\text{vir}}}{11} \right)^{-1} \text{ kpc.} \quad (\text{A2})$$

The virial temperature (T_{vir}) is estimated as

$$\begin{aligned} T_{\text{vir}} &\simeq \frac{G\mu' m_{\text{H}} M_{\text{vir}}}{3k_{\text{B}} r_{\text{vir}}} \\ &= 1.9 \times 10^5 \left(\frac{M_{\text{vir}}}{10^{10} M_{\odot}} \right)^{2/3} \left(\frac{1+z_{\text{vir}}}{11} \right) \text{ K,} \end{aligned} \quad (\text{A3})$$

where $\mu' m_{\text{H}}$ is the mean particle mass ($\mu' = 0.65$), and we used equation (2) from the first to the second line.

The cosmic age at high redshift is approximated by (e.g. Furlanetto et al. 2006)

$$t_0(z) \simeq \int_{\infty}^z \frac{dz'}{(1+z')H(z')} = 4.7 \times 10^8 \left(\frac{1+z}{11} \right)^{-3/2} \text{ yr,} \quad (\text{A4})$$

where $H(z)$ is the Hubble parameter at redshift z , which is approximated in the matter-dominated Universe at high redshift as $H(z) \simeq H_0 \Omega_{\text{m}}^{1/2} (1+z)^{3/2}$.

This paper has been typeset from a $\text{\TeX}/\text{\LaTeX}$ file prepared by the author.